Journal of Neural Engineering

PAPER

Estimation of seizure onset zone from ictal scalp EEG using independent component analysis in extratemporal lobe epilepsy

Aurélie de Borman[1,*], **Simone Vespa**[2], **Riëm El Tahry**[2,3] and **P.-A. Absil**[1]

[1] ICTEAM Institute, UCLouvain, Louvain-la-Neuve, Belgium
[2] Institute of Neuroscience (IoNS), UCLouvain, Brussels, Belgium
[3] Center for Refractory Epilepsy, Department of Neurology, Cliniques Universitaires Saint-Luc, Brussels, Belgium
[*] Author to whom any correspondence should be addressed.

E-mail: aureliedeborman@gmail.com

Keywords: independent component analysis (ICA), epilepsy, seizure onset zone, electroencephalogram (EEG), source imaging

RECEIVED
15 November 2021

REVISED
7 February 2022

ACCEPTED FOR PUBLICATION
16 February 2022

PUBLISHED
10 March 2022

Abstract

Objective. The purpose of this study is to localize the seizure onset zone of patients suffering from drug-resistant epilepsy. During the last two decades, multiple studies proposed the use of independent component analysis (ICA) to analyze ictal electroencephalogram (EEG) recordings. This study aims at evaluating ICA potential with quantitative measurements. In particular, we address the challenging step where the components extracted by ICA of an ictal nature must be selected. *Approach.* We considered a cohort of 10 patients suffering from extratemporal lobe epilepsy who were rendered seizure-free after surgery. Different sets of pre-processing parameters were compared and component features were explored to help distinguish ictal components from others. Quantitative measurements were implemented to determine whether some of the components returned by ICA were located within the resection zone and thus likely to be ictal. Finally, an assistance to the component selection was proposed based on the implemented features. *Main results.* For every seizure, at least one component returned by ICA was localized within the resection zone, with the optimal pre-processing parameters. Three features were found to distinguish components localized within the resection zone: the dispersion of their active brain sources, the ictal rhythm power and the contribution to the EEG variance. Using the implemented component selection assistance based on the features, the probability that the first proposed component yields an accurate estimation reaches 51.43% (without assistance: 24.74%). The accuracy reaches 80% when considering the best result within the first five components. *Significance.* This study confirms the utility of ICA for ictal EEG analysis in extratemporal lobe epilepsy, and suggests relevant features to analyze the components returned by ICA. A component selection assistance is proposed to guide clinicians in their choice for ictal components.

1. Introduction

About one third of epileptic patients suffer from drug-resistant epilepsy, meaning that despite adequate pharmacological treatment, control of seizures cannot be achieved [1]. In certain of those cases, surgery becomes an interesting option, with the aim to remove or disconnect the brain zone that generates the seizures [2]. In order to execute a successful surgery, it is essential to correctly localize the seizure onset zone [3]. This often requires the invasive placement of intracranial electrodes, in a procedure defined as stereo-electroencephalogram (EEG). However, the localizing potential of the non-invasive presurgical evaluation (i.e. phase I) may be enhanced by computational analyses of scalp EEG [4]. Improving the seizure onset zone localization at the end of phase I is of utmost importance, as this can lead to a better definition of intracranial targets for stereo-EEG, or enable directly a curative surgery in some cases [5].

During the last two decades, multiple studies have proposed the use of independent component analysis (ICA) to improve ictal EEG analysis in patients with intractable epilepsy. In the first place, ICA was mainly used to remove artifacts from ictal EEGs [6–8] and its

localization ability was limited to scalp maps [9, 10]. Nam *et al* proposed to apply ICA to the seizures of patients with medial temporal lobe epilepsy [10]. The lateralizing power of ictal EEG was proved to be increased thanks to the inspection of the scalp maps of components with ictal nature, i.e. ictal components. However, the idea to locate more precisely the derived components quickly arose with the emergence of electrical source imaging (ESI) techniques. Some studies proposed to use methods that compute a single dipole location that best explains a component activity [11, 12]. Other studies suggested the usage of distributed methods to either localize the back-projected activity of a single component [13] or multiple components at once [14, 15].

A challenging step in applying ICA to epilepsy is to identify which of the extracted independent components have an ictal nature. Most of the cited studies rely on visual inspection of the component signals. To support the visual inspection, Nam *et al* reviewed the auto-correlograms and also computed the portion of power in the 2–10 Hz bandwidth in order to help the component selection [10]. Other studies also considered event-related spectrum perturbation that allows a visual time-frequency analysis of the components [11, 12]. In the range of studies using distributed ESI methods, Yang *et al* [14] proposed a method to select the ictal components where they compute the correlations between time-frequency representations of each independent component and of the electrodes showing the most ictal activity in a reconstructed EEG. The method required some visual inspection to build the noise-deducted EEG (by identifying artefact components) and then to identify the electrodes showing ictal activity in the reconstructed EEG. More recently, Habib *et al* [16] proposed a recursive ICA-decomposition that requires a clinician's intervention only to specify the frequency of the ictal rhythm. The technique works by repetitively applying ICA, eliminating a component, and back-projecting the remaining components until a sufficiently satisfying component is obtained.

One way to assess the utility of ICA in assisting ictal EEG analysis would be to find out if there is at least one returned component per seizure that, if chosen, would lead to a correct estimation of the seizure onset zone. Furthermore, it would be of interest to determine whether such component(s) show some distinctive features, which could be exploited to guide the crucial step of choosing the ictal components. In this study, we aimed to evaluate ICA potential to correctly localize the seizure onset zone by verifying whether there are components located within the resection zone for each studied seizure. This could be done thanks to the co-registration of the component origins (computed by ESI) and the so-called epileptogenic zone, estimated by the resection zone of patients who underwent surgery and became seizure-free. Particularly, we addressed a population of extratemporal lobe epilepsy patients. In this epilepsy type, ictal EEG analyses are renowned to be more challenging compared to temporal lobe epilepsy (e.g. shorter seizures, less rhythmical patterns, lower signal-to-noise ratio due to major movement artifacts) [17], and have so far been object of a minority of ICA studies. Our analysis was performed with multiple pre-processing parameters (different filters and time windows) in order to assess how to preprocess the signals to obtain the most favorable outcome. In addition, we computed and analyzed a series of quantitative features for each of the components returned by ICA. We were able to objectively evaluate whether the components located in the resection zone differ from those that are outside the zone. To the best of our knowledge, this is the first time that a quantitative analysis of the components returned by ICA and of their underlying characteristics is performed. Features that were significantly different between the components located inside and outside the resection zone were used to design an algorithm assisting the ictal component selection. This selection assistance is embedded into a structured pipeline describing the procedure to apply ICA to ictal EEG starting from the raw recordings and leading to the estimated onset zone. Preliminary results of this study appeared in the thesis [18].

2. Methods

2.1. Patients and recordings

This study was conducted using anonymized retrospective data and was approved by the Institutional Review Board of Saint-Luc University Hospital, Brussels, Belgium 2018/25JAN/030. The EEG signals were recorded at Saint-Luc University Hospital and at Centre Neurologique William Lennox, Ottignies, Belgium. Between 19 and 23 electrodes were available for each patient but only the 19 electrodes placed according to the International 10–20 system [19] were used for the sake of homogeneity. The sampling rate was 256 Hz. Structural MRI scans were performed with a with a 1.5 T or 3.0 T scanner (Siemens, Erlangen, Germany), and 3D volumetric T1-weighted magnetization-prepared rapid acquisition with gradient echo (MPRAGE) sequences were used.

To be included in this study, patients had to satisfy the following inclusion criteria:

(a) The patient suffers from drug-resistant extratemporal focal epilepsy.
(b) A curative epilepsy surgery (lesionectomy, disconnection, hemispherotomy) was performed.
(c) Long-term scalp EEG monitoring (of at least 24 h) and post-operative structural MRI are available.
(d) The post-operative follow-up lasted at least one year.

Table 1. Clinical data details: the rightmost column indicates the frequency band characterizing the epileptic activity, the number in parenthesis indicates the number of seizures with such a rhythm.

Patient	Number of seizures	Epilepsy location	Type of surgery	Ictal frequency band
1	3	Right frontal lobe	Disconnection	Theta-alpha
2	5	Right temporo-occipital lobe	Disconnection	Alpha
3	2	Plurifocal left hemisphere	Hemispherotomy	Delta (1), theta (1)
4	5	Plurifocal left hemisphere	Hemispherotomy	Theta
5	5	Plurifocal right hemisphere	Hemispherotomy	Delta (1), theta (4)
6	4	Right frontal lobe	Disconnection	Delta-theta (1), theta-alpha (3)
7	2	Left temporo-occipital lobe	Disconnection	Theta
8	1	Plurifocal right hemisphere	Hemispherotomy	Beta
9	4	Right parieto-occipital lobe	Disconnection	Delta (1), theta (2), delta-theta (1)
10	4	Right frontal lobe	Lesionectomy	Alpha

(e) The patient became seizure-free after surgery (ILAE class 1 [20]).
(f) At least one recorded seizure shows rhythmic activity.

According to these criteria, 10 patients were selected from the database of the Centre for Refractory Epilepsy of Saint Luc University Hospital. Because this study relies on the rhythmic nature of seizures, only seizures labeled as 'rhythmic' by neurologists were included for the analysis. This left us with a total of 35 seizures (out of 51 seizures). Neurologists identified for each seizure a frequency band characterizing the epileptic activity. Details about the clinical data can be found in table 1.

2.2. Pipeline overview

The proposed analysis relies on the construction of a structured pipeline having as input the EEG file capturing the seizure while the output is an estimation of the seizure onset zone within a 3D brain model. A graphical representation of the pipeline can be seen in figure 1. All codes were written in Matlab using the EEGLAB toolbox [21].

2.2.1. Step 1: data pre-processing

EEG segments of 1 h length, containing the seizure(s) as previously annotated by a neurologist, were uploaded and pre-processed using two types of digital filters: a notch filter (49–51 Hz) and a band-pass filter aiming to isolate genuine brain activity. Both filters were designed using fourth-order Butterworth filters. The upper cutoff frequency of the band-pass filter was set to 30 Hz to avoid including muscular activity, often present during seizures, which frequency range is particularly predominant above 30 Hz [22]. Multiple lower cutoff frequencies were compared. Previous studies applying ICA to ictal EEG used high-pass filters with a cutoff frequency varying from 0.3 to 1 Hz. With the purpose of eliminating artefacts using ICA, the influence of high-pass filtering was studied by Winkler *et al* [23] and they showed that high-pass filtering between 1 and 2 Hz consistently achieved good results in terms of signal-to-noise ratio and percentage of 'near-dipolar' ICA components. Accordingly, we compared lower cutoff frequencies of 1 and 2 Hz. At this point, corrupted electrodes were manually rejected. No more than two electrodes were removed per seizure. The last pre-processing step consisted in re-referencing the data against a common average [24].

2.2.2. Step 2: time window selection

Before applying ICA, the time window that will be used by the algorithm for the extraction of ictal components must be chosen. In this study, markers were placed by experienced neurologists to indicate the seizure onsets. Therefore, it remained to choose how many seconds before and after the markers would be submitted to ICA. A proportion of one third before and two third after onset was chosen to include background activity before seizure. A tradeoff between narrow (to avoid inclusion of seizure propagation or artifacts) and longer windows (allowing that a sufficiently large dataset is included for parameter learning) was sought. A rule of thumb suggests that at least $N^2 \times k$ data points should be given to ICA for EEG data where N is the number of electrodes and k is a multiple, typically equal to 20 [25]. In this study, 19 electrodes were used with a sampling rate equal to 256 Hz, meaning that a window of approximately 28 s should be given to ICA, taking k equal to 20. In order to investigate the above-mentioned tradeoff, shorter time windows were also considered. The studied pre-processing parameters are summarized in table 2.

2.2.3. Step 3: ICA decomposition

ICA is the key element of the proposed pipeline. Let $\Phi \in R^{N\times T}$ denote the recorded EEG data, where N is the number of channels and T the number of time samples. An ICA algorithm returns a weight matrix $W \in R^{N\times N}$ such that the N signals in $X = W\Phi$, termed *components*, are as independent as possible from each other [26–28]. EEGLAB proposes several ICA algorithms to apply to EEG data, relying on different measures of independence. In this pipeline, we apply the most commonly used algorithm for seizure analysis: the Extended Infomax algorithm [29, 30].

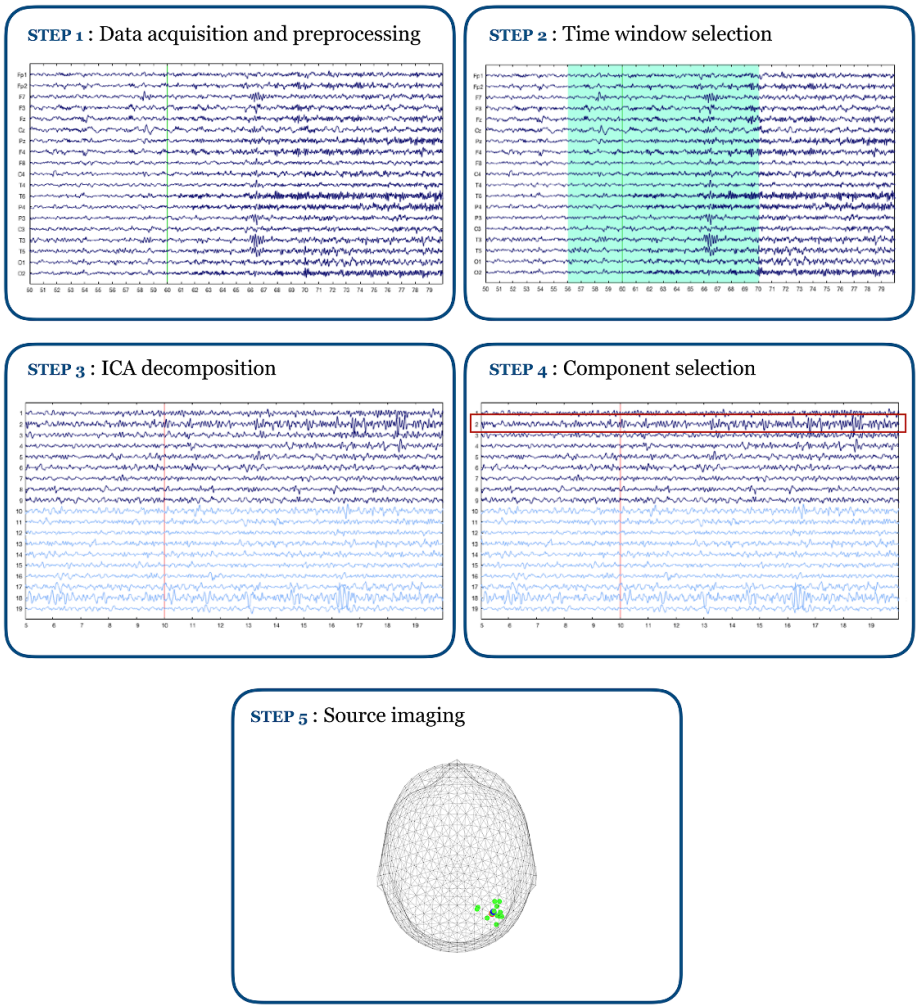

Figure 1. Pipeline overview.

Table 2. Studied pre-processing parameters. The last two rows correspond to the number of seconds before and after the seizure marker that were selected for the analysis.

Setup	a	b	c	d	e	f
High-pass (Hz)	1	2	1	2	1	2
Before (s)	2.5	2.5	5	5	10	10
After (s)	5	5	10	10	20	20

2.2.4. Step 4: component selection

Once the ICA algorithm has computed the N independent components, it crucially remains to determine which are the components that isolate seizure activity. These components will then be further considered in order to locate the seizure onset zone. First, we analyzed whether there is for each seizure at least one component that would lead to a correct estimation of the seizure onset zone (using source imaging, as explained in the next paragraph). Next, features were implemented and analyzed for each of the components. These features are described in section 2.3. Since components can be localized using source imaging, it was possible to analyze whether the features of the components located within the resection zone differ from those of other components (see section 2.6). In light of the feature analysis, a component selection assistance was constructed taking into account the most relevant features. The process consisted of two steps: (1) rejection of components having features that do not satisfy some thresholds, (2) sorting of the accepted components according to a feature. The algorithm is therefore conceived to assist a clinician in his/her choice for ictal components.

2.2.5. Step 5: source imaging

In order to localize the origin of the extracted components within the brain, source imaging is performed using the exact low-resolution electromagnetic tomography (eLORETA) method [31, 32]. The implementation of the source imaging step relies on codes made available in the context of a study

analyzing functional connectivity and following ESI in simulated EEG [33, 34]. The standard lead field matrix of the New York head (ICBM-NY) [35] was used and the regularization parameter for eLORETA was set to 0.01. In the specific context of the pipeline, the activity of components obtained by ICA must be localized. To do so, the activity of the component(s) must first be back-projected at the level of the electrodes before applying eLORETA. This back-projection can simply be done using the inverse of the weight matrix W given by ICA. The back-projection of component i is computed as $\Phi_i = w_i^{-1} x_i$ where w_i^{-1} is the ith column of W^{-1} and x_i the ith row of X. To determine what source points are the most active, the levels of activity are given by the coefficients of the vector Pw_i^{-1} where P is the spatial filter derived by eLORETA. These values were normalized between 0 and 1 by dividing by the maximum level. All the source points having an activity above 0.8 were called the *active cloud* and formed the output of the pipeline.

2.3. Ictal component feature analysis

As mentioned above, a series of features for each of the components were computed and studied with the purpose of recognizing components isolating seizure activity, and thus leading to an accurate estimation of the seizure onset zone. The goal was to describe mathematically attributes that we expected to differ between ictal and non-ictal components. At this point, we should point out that ICA has a scaling indeterminacy: if a component x_i is scaled by α (and w_i^{-1} scaled by $\frac{1}{\alpha}$ in order to preserve the backprojected component Φ_i), then its independence from the other components is preserved. In view of this, the implementation was made in such a way that the scale of the components does not impact the features.

2.3.1. Dispersion measure

For each component, it is possible to back-project the activity of the component alone and then apply ESI to obtain the active cloud (most active brain source points). The first feature that was implemented is the dispersion of that active cloud. In theory, an ictal component should isolate an activity generated by a specific population of neurons. Therefore, if a component leads to a diffuse active cloud, it is unlikely that the component isolates seizure activity because the seizure onset zone is supposed to be focal. Several implementations are possible to compute the dispersion of a cloud of points. We decided to compute the Frobenius norm of the covariance matrix of the 3D coordinates.

2.3.2. Ictal rhythm power

The next feature is the percentage of spectral power in the ictal frequency band. The motivation behind this feature lies in the fact that the seizures are rhythmic and therefore the components that isolate seizure activity should be sufficiently rhythmic. This feature required a neurologist to identify the frequency band of the ictal rhythm. Instead of simply looking at the average power in the ictal frequency band, it is the percentage of power that was computed by calculating the ratio of the average power in the ictal frequency band and the total power of the component signal. Doing so, issues with the scaling of the components were avoided. Indeed, if a component signal is multiplied by a factor α, its average power in the frequency band is multiplied by α^2 while the percentage remains the same.

2.3.3. Broadband physiological power

The next feature is somewhat similar to the previous feature, except that the frequency range taken into account is broader: from 2 to 20 Hz. The motivation behind it is that seizures included in this study, and more generally the majority of rhythmic seizures seen at scalp, have their activity comprised in that frequency range [17]. Moreover, artefactual or spurious non-electrocerebral activities are more likely to lie outside the 2–20 Hz broadband range compared to genuine brain rhythms. This feature is more robust than the previous one in the sense that it does not rely on a clinician's choice. However, this broader frequency range could also correspond to physiological non-ictal brain activities. To avoid troubles with the scaling, the feature was implemented similarly to the previous one as a percentage of power in the frequency band 2–20 Hz.

2.3.4. EEG variance contribution

We also explored to which extent each component contributes to the EEG variance in the analyzed time window. We expect that a component accounting for seizure activity should contribute significantly to the EEG variance. It allows gaining knowledge about how predominant a component is, despite the scaling indeterminacy. Its implementation was inspired by the *eeg_pvaf* function from the EEGLAB toolbox. This function computes what they call the percent variance accounted for. However, we will talk about EEG variance contribution as the value could be negative due to the fact that the computed components are not exactly orthogonal. A negative value means that by removing the component activity the EEG variance increases. We expect this kind of situation to be very unlikely for components that isolate seizure activity since it is not in accordance with the concept of a component isolating a real physiological phenomenon. The feature needs to compute the ratio of the variance of the EEG without the component and the variance of the initial EEG. To remove a component contribution, its signal is back-projected at the level of the electrodes using the inverse of the weight matrix and then removed from the EEG. The equation behind the feature is presented hereunder (the operator *var* denotes the mean of the row-wise variances):

$$feat = 1 - \frac{var\left(\Phi - backproj\left(x_i\right)\right)}{var\left(\Phi\right)} = 1 - \frac{var\left(\Phi - w_i^{-1}x_i\right)}{var\left(\Phi\right)}.$$

2.3.5. Change of variance

Another proposed feature is the change of variance observed at the seizure onset. So far, the features were computed over a period of 10 s after the seizure marker. This feature attempts to take advantage of the fact that the seizure should start at the marker indicated by the clinician. A component that isolates seizure activity should have its variance that increases during the period after the onset in comparison with the period before the onset. To avoid any issues with the scaling, the feature was implemented by taking a ratio: the variance after the onset is divided by the variance before the onset. Doing so, we expect a larger value for ictal than non-ictal components.

2.3.6. Change of entropy

A last feature that was analyzed is the change of entropy at the onset. The entropy of a signal is a measure of its uncertainty. A high entropy typically means that the signal is hardly predictable. The motivation behind the feature lies in the fact that brain activity is thought to be more predictable during a seizure than it usually is [36]. Thus a drop of entropy could be observed at the onset marker in components isolating seizure activity. The spectral entropy was computed before and after the marker onset. Spectral entropy was computed as the Shannon entropy of the spectral power distribution in the frequency domain. Since the entropy of a signal does not depend on its scale, the feature was simply implemented as a difference of entropy after and before the marker. A negative value would therefore mean that the entropy has dropped.

2.4. Validation: co-registration and subsequent component localization

All patients included in this study became seizure-free after surgery. Accordingly, the seizure onset zone is assumed to be located inside the resection zone. It is then of interest to measure the distance and overlap between that region and the estimated zone given by the pipeline, and particularly at a single component-level. Indeed, to analyze ICA potential while avoiding a subjective component selection, each of the components was localized separately making it possible to count the number of components lying within the resection zone for each seizure. MRI scans were first normalized using the SPM12 toolbox [37] in order to match the head model used by source imaging. Next, the resection zones were drawn manually on the post-operative scans under the supervision of experienced medical staff, with the help of a tool that draws 3D shapes based on voxel intensity [38].

Three quantitative measures were implemented to objectively determine which components lied in the resection zone: (1) the Euclidean distance between the border of the resection zone and the most active source point, (2) the Euclidean distance between the borders of the resection zone and the average position of the active cloud (i.e. source points having a large enough activity level) and (3) the percentage of source points belonging to the active cloud that are located inside the resection zone. A component was considered as *accurate* (i.e. lying within the resection zone) if: (1) the most active point of the active cloud was sufficiently close to the resection zone, (2) the average position of the active cloud was sufficiently close to the resection zone and (3) the percentage of active cloud inside the resection zone was sufficiently high. Since the type of performed surgery influences the tolerance that may be allowed in the localization error, we decided to set this limit at 1 cm for all patients, except for those who underwent a lesionectomy, for which tolerance was set to 2 cm. The percentage of active cloud inside the resection zone had to be higher than 90% for hemispherotomies, 70% for disconnections and at least one point of the active cloud must be within the resection zone for lesionectomies.

2.5. Performance measurement: pre-processing parameters

We proceeded as follows to select the setup among those in table 2. For each seizure, the number of accurate components (i.e. lying within the resection zone) was counted using the criteria established above. Nevertheless, having numerous components lying in the resection zone is not necessarily better than having a single component that is correctly localized. In fact, in the second case, the seizure activity was probably isolated in one single component which is more desirable than having the activity spread over multiple components. Therefore, the performance of pre-processing parameters was evaluated according to the number of seizures for which at least one component was located within the resection zone rather than the number of components having their source in the resection zone. This analysis was conducted for each of the pre-processing parameters presented in table 2. Two additional criteria on the components' characteristics were used to discern what pre-processing parameters should be chosen. First, it is not desirable to consider as accurate a component that leads to a diffuse active cloud within the brain. Therefore, components having a dispersion exceeding a given limit ($\geqslant 500$ mm^2) were not considered as accurate anymore. Second, since seizures considered in this study are rhythmic, only components showing a sufficient spectral content in the pre-determined frequency band of interest ($\geqslant 20\%$) were still considered as accurate. This could be done thanks to the ictal rhythm power feature. The rest of the analysis was performed using the pre-processing parameters yielding the best performance.

2.6. Statistical analysis of the features

We termed as accurate those components that satisfied the criteria related to the localization of the active cloud, listed in section 2.4. Statistical analyses were carried out to distinguish accurate from non-accurate components. For each feature, we extracted the mean, median, standard deviation and interquartile range values. Boxplots were displayed for both accurate and non-accurate components to gain insight into the distribution of the values. Next, statistical tests were conducted to further assess the difference between the two groups. Depending on the feature distribution, either a t-test or Wilcoxon rank-sum test was performed (significance at $p < 0.05$). A Kolmogorov–Smirnov test was conducted to evaluate whether the distribution is likely to be normal (significance at $p < 0.05$) and decide if a t-test is suited.

Additionally, receiver operating characteristic (ROC) curves were created to assess whether a threshold on the feature would allow to discriminate between accurate and non-accurate components. Note that the curves were plotted with the specificity on the x-axis and the sensitivity on the y-axis. The proposed component selection assistance consists in first rejecting components whose features do not satisfy some thresholds. Therefore, we analyzed the ROC curve and highlighted the value of specificity corresponding to 90% sensitivity (that we term as *rejection quality*). If this value is greater than 10% it means that the ROC curve detaches from a random binary classification and that choosing the corresponding threshold for the feature allows to get rid of non-accurate components while keeping the majority of accurate components. Thresholds of the selection assistance were set at the value corresponding to 90% sensitivity on the ROC curve. The value of 90% was chosen since high sensitivity is desirable to avoid eliminating accurate components.

2.7. Performance measurement: component selection assistance and seizure onset zone localization

Two types of analysis were conducted to assess the quality of the component selection assistance and more generally of the final ICA + ESI pipeline. On the one hand, a seizure-based analysis was carried out, taking into account the percentage of seizures for which the first proposed components are accurate. On the other hand, we also performed a component-based analysis that considers the components regardless of their associated seizures, e.g. the percentage of components that are accepted overall seizures. From a clinical point of view, the first analysis is the most relevant. Indeed, to estimate the ICA algorithm potential it is essentially needed to have at least one accurate component per seizure which, if appropriately identified, might lead to successful seizure onset zone localization. However, the component-based analysis gives a general picture of what the selection process achieved. The component selection assistance we propose relies on a few parameters, i.e. the thresholds set to reject components in the first step. These must be learned from the dataset and therefore we performed a leave-one-patient-out validation in order to diminish the risk of overestimating the performance on new data. Thresholds were thus computed based on the features of all the patients, except the one on which we want to assess the performance.

3. Results

3.1. ICA optimal pre-processing parameters

The first line of table 3 presents the percentage of seizures for which at least one component led to a correct position (using the criteria stated in section 2.4). Interestingly, the proportion is high for each of the setups and no significant difference was observed using only criteria on the location of the active cloud. Table 3 presents the percentage of seizures for which at least one component was accurate according to the different sets of quality criteria as explained in section 2.5. Overall, we observe that setup f performs slightly better than the other setups. For any set of quality criteria, setup f achieves the best performance, reaching 100% for the first two sets. Consequently, it was decided to proceed to the analysis of the pipeline using that setup.

3.2. Feature analysis

Table 4 and figure 2 summarize the results of the feature analysis. Boxplots and ROC curves are only displayed for the features that were shown relevant for the component selection assistance.

3.2.1. Dispersion measure

We observed that the mean of the feature is smaller for accurate components than for non-accurate components. That is in accordance with the expectations because well-located components are likely to isolate seizure activity originating from a limited brain region. A Wilcoxon rank-sum test was performed since the distribution is unlikely to be normal ($p > 0.05$ for the Kolmogorov–Smirnov test), preventing the use of a classical t-test. The Wilcoxon rank-sum test was significant, suggesting that it is unlikely that both accurate and non-accurate groups come from the same distribution. The ROC curve (figure 2(d)) detaches from the random classification meaning that it could benefit a classification process.

3.2.2. Ictal rhythm power

As expectable, the mean value of the feature is larger for accurate components than for non-accurate components, and it was confirmed by a significant t-test. This feature shows the greatest area under the curve (AUC, figure 2(e)) and rejection quality while it still does not suggest that the feature alone could perfectly

Table 3. Comparison of performance between the set of parameters presented in table 2. Performance is computed as the percentage of seizures for which at least one component fulfills the criteria with a checkmark. Location refers to the criteria stated in section 2.4 related to the position of the active cloud with respect to the resection zone. Dispersion and rhythmicity refers to the criteria explained in section 2.5.

	Quality criteria			Setups					
	Location	Dispersion	Rhythmicity	a	b	c	d	e	f
1	✓			97.1%	97.1%	94.3%	94.3%	94.3%	100%
2	✓	✓		94.3%	94.3%	94.3%	91.4%	94.3%	100%
3	✓	✓	✓	85.7%	88.6%	91.4%	85.7%	91.4%	97.1%

Table 4. Feature analysis. The mean and standard deviation of each feature are given for both accurate and non-accurate components. Components are considered as accurate based on the location criteria stated in section 2.4. The p-value is associated to a t-test (for the ictal rhythm power and the change of entropy) or a Wilcoxon rank sum test (for the other features) and assess the difference between accurate and non-accurate component features. The last line (rejection quality) indicates the specificity at 90% sensitivity.

		Dispersion (mm^2)	Ictal rhythm power (%)	Broadband physiological power (%)	EEG variance contribution (%)	Change of variance	Change of entropy
Mean	Accurate	416.63	36.63	91.56	6.28	3.1152	−0.0102
	Non-accurate	569.89	30.50	90.40	5.30	4.5474	0.0210
Standard deviation	Accurate	463.19	12.07	7.37	6.19	7.8037	0.6087
	Non-accurate	673.53	13.42	7.47	6.55	13.2111	0.5895
p-Value		3e-04	2e-07	0.0035	0.0110	0.0878	0.5611
Rejection quality		19.79%	29.90%	10.10%	16.08%	10.72%	11.55%

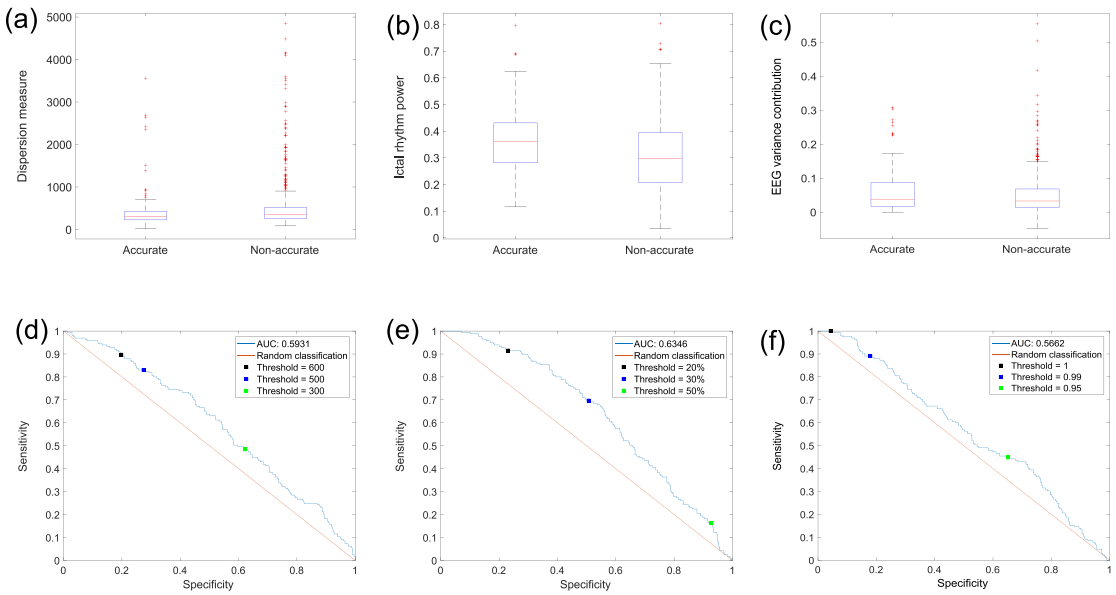

Figure 2. Boxplots (a) dispersion measure, (b) ictal rhythm power and (c) EEG variance contribution. The red line indicates the median. The bottom and top edges of the box indicate the 25th and 75th percentiles, respectively. The red crosses mark the outliers and the black lines indicate the presence of data points not considered as outliers. ROC curve for (d) dispersion measure, (e) ictal power frequency and (f) EEG variance contribution.

discriminate between the accurate and non-accurate components.

3.2.3. Broadband physiological power

Overall, the difference between accurate and non-accurate components is not striking for this feature. The mean is slightly higher for accurate components as expected but the variation is rather small. The Wilcoxon rank sum test ($p < 0.05$ for the Kolmogorov–Smirnov test) shows that there is a difference between accurate and non-accurate components yet the *p*-value is higher than for the previous features. The rejection quality value is very close to 10%, indicating a poor chance to discriminate accurate and non-accurate components using a threshold.

3.2.4. EEG variance contribution

The mean of the feature is larger for accurate components than they are for non-accurate components. Hence, ictal accurate components were shown to impact significantly more the EEG variance than the non-accurate ones as confirmed by a Wilcoxon rank-sum test ($p < 0.05$ for the Kolmogorov–Smirnov test). Finally, the box plots confirm that no accurate components reach a negative value while this happens for non-accurate components. The ROC curve detaches from the random classification (figure 2(f)).

3.2.5. Change of variance

Contrary to our expectations, the mean were slightly larger for non-accurate than for accurate components. The Wilcoxon rank sum tests and rejection quality value did not suggest that the feature was relevant to analyze further.

3.2.6. Change of entropy

We observed that the mean is negative for accurate components while being positive for non-accurate components, as we had expected. However, both means are very close to zero. The p-value of the t-test indicates that there is no significant difference between accurate and non-accurate components.

3.3. Component selection assistance

Based on the feature analysis, the component selection assistance of the pipeline could be designed. The first step consisted in rejecting components whose feature values do not reach certain thresholds, which were established based on the ROC curve analysis, as explained in section 2.6. The features that did not yield a significant difference (see p-values in table 4) between the accurate and non-accurate components were not employed, i.e. the change of variance and change of entropy. Moreover, the physiological power feature was not used because the rejection quality value was too close to 10%, i.e. too close to a line of no effect. In a nutshell, the features that served the selection assistance were: the dispersion, the ictal rhythm power and the EEG variance contribution. The second step of the process was designed to sort the accepted components according to a particular feature. Considering the previous analysis, the feature that showed the smallest p-value and largest rejection quality (i.e. the most distinctive of ictal accurate components) was chosen: namely the ictal rhythm power.

3.4. Seizure onset zone localization performance

Table 5 summarizes the results for both seizure- and component-based analysis. The results are presented for patients with a limited resection only (disconnection and lesionectomy) and all patients (including hemispherotomy). The selection and sorting of components allowed the first component to be accurate in 10/22 seizures (45.45%) for limited resection patients and in 18/35 (51.43%) considering all patients. In comparison, this probability drops to 16.68% and 24.74%, for limited resection patients and all patients, respectively, if components are sorted randomly and without rejecting components (the experiment was repeated 100 times). We also observe that the probability that at least one component is accurate within the 5 first components reaches 80% in both subgroups. Two examples of seizures analyzed with the proposed algorithm are provided in figures 3 and 4. For more details on the performance of the sorting process, table 6 presents the sorted position of the first accurate component for each of the seizures.

Moreover, when looking at the efficacy of the rejection process itself, we observe that there is almost a 95% chance that at least one accurate component was kept. In terms of number of seizures, only 2 out of 35 seizures had no accurate component among the accepted components. The component-based analysis shows how many components were accepted overall. Approximately half of the components are kept. Another possibility to estimate the efficiency of the selection process was to determine the percentage of components that was accurate before and after the rejection step. There is a substantial 11.32% increase of the percentage after the selection process for the patients who underwent a limited resection, and a 9.40% increase for all patients.

4. Discussion

This study aimed at estimating the seizure onset zone from ictal low-density EEG using advanced computational techniques: namely, ICA and ESI. A pipeline was implemented to reach that goal and to structure the work. Quantitative measures allowed us to objectively analyze the pipeline performance while many studies in the field of ICA applied to ictal EEG rely on visual inspection to validate their results. This was possible thanks to the co-registration of the pipeline output and the resection zone in patient-specific MRIs. The results show that for every analyzed seizure and with the optimal pre-processing parameters (i.e. setup f, see table 2) there is at least one component that, if chosen, would lead to a position inside the resection zone. This confirms the utility of ICA and source imaging with the purpose of estimating the seizure onset zone.

We compared different pre-processing parameters since there is no consensus about these choices in the literature. Our results suggest that ICA is robust to the choice of pre-processing parameters, given the high performance for all of the studied setups (see table 3). By refining the analysis, we came to the conclusion that using the longest time window with a 2 Hz high pass filter would yield the best outcome.

Table 5. Component selection performance. For the seizure-based analysis, the number of seizures satisfying the condition in the left column is specified as well as the percentage it represents, both for limited resection and all seizures. For the component-based analysis, percentages of number of components are given.

	Limited resection	All
Seizure-based		
First component is accurate	10/22 (45.45%)	18/35 (51.43%)
At least one accurate component:		
Within the 3 first components	14/22 (63.64%)	25/35 (71.43%)
Within the 5 first components	18/22 (81.82%)	28/35 (80.00%)
Within the accepted components	21/22 (95.45%)	33/35 (94.29%)
Component-based		
Percentage of accepted components	42.33%	53.08%
Percentage of accurate components:		
Within all components	17.33%	25.38%
Within accepted components	28.65%	34.78%

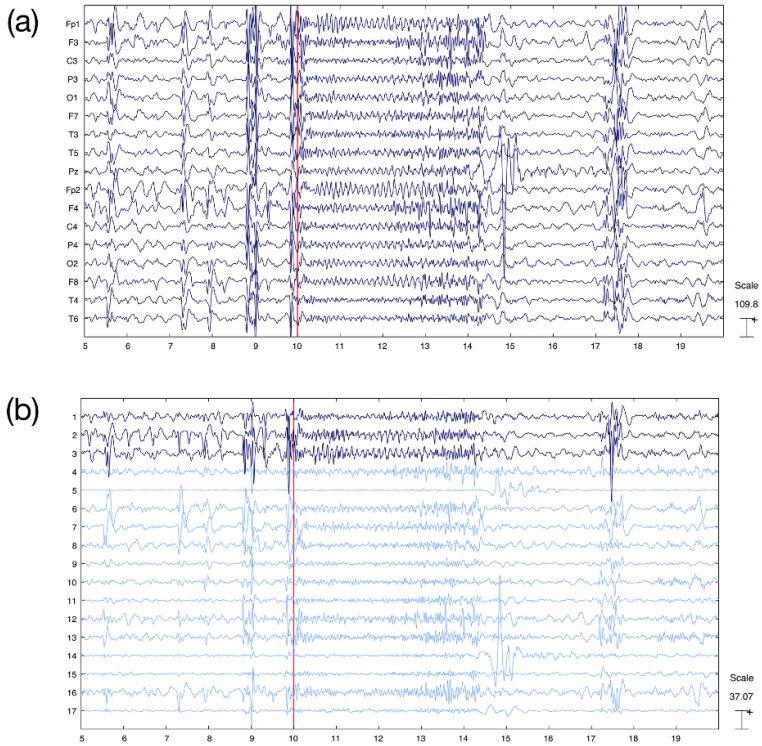

Figure 3. First seizure of patient 1. Example of pipeline application. (a) The EEG epoch containing the seizure is displayed (10–20 system electrodes, common average referencing). The seizure onset timing was marked by the epileptologists (red vertical line). A tonic seizure, of approx. 5 s duration, can be distinguished. It visually presents with a theta/alpha rhythmical activity with highest voltages seen bilaterally over Fp1 and Fp2 electrodes. (b) The components returned after application of the ICA (with the optimal pre-processing parameters) and of the component selection pipeline are displayed. The accepted components can be seen in dark blue. The rejected components are listed thereafter, and can be seen in light blue. (c), (d) The active clouds of the first two sorted components are displayed after co-registration in comparison with the resection zone, in the patient-specific MRI. The first component is localized near the posterior boundary of the resection zone (average within 2 cm), while the second shows the totality of the active cloud, its average and maximum within the resection zone. The resection zone is shown in orange and a tolerance of 1 cm (not displayed in orange) was set to determine whether a source point lies within that region.

This is in accordance with the rule of thumb mentioned in section 2.2 [25] and the assumption that ICA is perturbed by low frequencies [23]. While the longest time window benefits the learning of ICA parameters, it might also be the case that the pre-ictal phase contains valuable information for the seizure onset zone estimation.

Many studies applying ICA to ictal EEG consider a majority of temporal lobe epilepsy patients [7, 9, 10, 12, 14, 16]. In this study, all of the patients suffered from extratemporal lobe epilepsy, known to be less rhythmical and with a lower signal-to-noise ratio. This study demonstrates that ICA might yield a correct estimation of the seizure onset zone even for

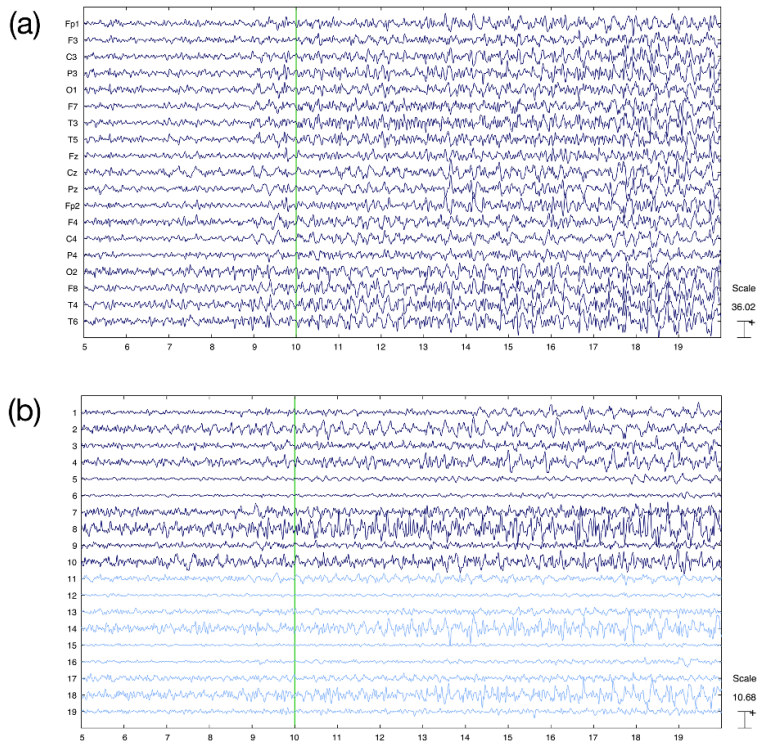

Figure 4. Second seizure of patient 9. Example of pipeline application. (a) The EEG epoch containing the beginning of the seizure is displayed (10–20 system electrodes, common average referencing). The seizure onset timing was marked by the epileptologists (green vertical line). A rhythmical activity, poorly localizable over single scalp electrodes, is seen building up, with delta waves predominating over the posterior regions. (b) The components returned after application of the ICA (with the optimal pre-processing parameters) and of the component selection pipeline are displayed. The accepted components can be seen in dark blue. The rejected components are listed thereafter, and can be seen in light blue. (c), (d) The active clouds of the first two sorted components are displayed after co-registration in comparison with the resection zone, in the patient-specific MRI. The active cloud of the first component overlaps with the anterior part of the resection zone while the totality of the active cloud of the second component is localized within the resection zone. The second component signal shows a clear rhythmicity attributable to seizure activity in view of the location. The resection zone is shown in orange and a tolerance of 1 cm (not displayed in orange) was set to determine whether a source point lies within that region.

Table 6. Patient-based analysis: for each seizure, the number indicates the sorted position of the first accurate component. Symbol 'X' indicates that no accepted component was accurate. A patient number in bold font indicates that the patient underwent a hemispherotomy.

Patient \ Seizure	1	2	3	4	5
1	2	X	1	—	—
2	1	1	1	1	1
3	10	X	—	—	—
4	1	1	1	2	1
5	1	2	2	1	1
6	8	5	3	5	—
7	6	3	—	—	—
8	1	—	—	—	—
9	2	1	1	1	—
10	1	4	7	8	—

extratemporal lobe epilepsy. While this study relies to some extent on seizure rhythmicity, the methodology does not aim to depend on rhythmicity exclusively. Features applicable for any type of seizure (i.e. dispersion and impact on EEG variance) were implemented and analyzed to take into account that seizures do not always exhibit a clear rhythmicity. If more features were implemented, it might even be possible to drop the rhythmicity-dependent feature, this way getting rid of the frequency-band-of-interest selection and expanding the applicability of the method to non-rhythmical seizures.

Co-registration of the pipeline output and the resection zone made it possible to analyze objectively and quantitatively the components returned by ICA. Instead of having to visually determine whether a component is localized within the resection zone, quantitative measures (distance in mm) allowed us to

objectively evaluate the distance and overlap between the resection zone and the pipeline output. While computing such a distance has already been reported in the literature [14, 15], it had only been used to assess the final performance of methods (which relied on visual inspection). In this study, we used the quantitative measures not only to evaluate the final performance but also to analyze each of the components returned by ICA. Indeed, we were able to categorize the components as accurate or non-accurate depending on their presumed source corresponding to the epileptogenic zone. The components reflecting electrical activities localized to the resection zone showed particular features which make them attributable to genuine ictal activity. They proved to be generally less diffuse, more rhythmical in the presumed band of interest and contribute sufficiently to the EEG variance compared to non-accurate components, which might instead represent either physiological or artefactual activity. These observations support the assumption that ICA is able to isolate seizure activity.

Three of the implemented component features were not employed by the component selection assistance: the broadband physiological power, the change of variance and the change of entropy. The physiological power was significantly different for accurate and non-accurate components. However, setting a threshold on that feature it was proved not to be efficacious with the purpose of a rejection process, and thus not suited for the component selection assistance we propose. For the change of variance feature, the mean was larger for non-accurate than for accurate components, against our expectations. This can be explained by the fact that components isolating artefacts could also show a large change of variance. A typical component isolating a movement artefact is flat except during the movement. Therefore, if the movement occurs after the seizure onset (which is likely) then the feature will be very large even though the component is not accurate. While entropy has been shown to be relevant in the field of EEG seizure detection [36, 39], the feature does not seem beneficial in the context of our pipeline. A potential explanation to this is that a component that perfectly isolates seizure activity should show little activity before the onset. Therefore, the signal should be almost constant before the onset meaning it has a very low entropy. Consequently, it makes sense that a component that isolates seizure activity will not necessarily show a drop of entropy.

The selected designed features can be compared with similar concepts found in the literature. In another study, Nam *et al* analyzed the rhythmic behavior of components by computing the proportion of the 2–10 Hz power for patients suffering from medial temporal lobe epilepsy [10]. In a similar way, the ictal rhythm power feature in our study targets the precise frequency band of seizure activity since rhythms are more variable in extratemporal lobe epilepsy. In another study [12], the residual variance of components (i.e. how well a dipole fits the data) was used to analyze the components returned by ICA. Components having a too high residual variance were rejected since this means the activity is unlikely to originate from a single dipole. While that measure applies to single dipole fitting methods, the dispersion feature extends the concept to distributed ESI methods. Accordingly, a component with a low residual variance is likely to have a low dispersion feature. Finally, a similar measure as the EEG variance contribution was implemented in EEGLAB [21] and we demonstrated that this feature could also benefit the component selection assistance.

The relevant features were used to implement a component selection assistance that orders the components in a way that the most likely to be ictal is sorted at the top. The probability that the first component is accurate was shown to be far superior than with a random ordering, increasing from 16.68% to 45.45% and 24.74% to 51.43% for limited-resection patients and all patients, respectively. These substantial increases prove the efficiency of the selection assistance. While the performance does not suggest to use the assistance as an automated component selection, we demonstrated that the probability that there is at least one accurate component within the first 3 or 5 components is remarkably high (respectively 64%–71% or 80%–83%). Therefore, the assistance may be intended as a guidance for the clinician to analyze the first few components rather than ensuring the first component is accurate. In addition, the component rejection allows for halving the number of components that a clinician needs to analyze, against a minimal loss of potentially accurate sources (which occurred only in 2/35 seizures). Two examples are provided in the previous section to illustrate situations a clinician would have to deal with by applying the pipeline. The clinician remains free to inspect the components and their brain origins while being guided by the selection assistance. The study aimed at using ICA in its simplest but powerful form, keeping the methodology intuitive. In a similar way that time-frequency representations are now commonly used for EEG analysis, ICA might offer one more promising perspective to inspect ictal EEG signals, increasing the chance of successful seizure localization and, potentially, of epilepsy surgeries.

This study was conducted with 19-channel EEG recordings. While it is evident that high-density EEG recordings have a better spatial resolution, it remains of interest to show the potential of low-density EEG. In fact, practicality issues may arise for patients to wear a high-density EEG cap during a long time period, which is generally needed for recording seizures and their relative ictal EEG. On the other hand, all epilepsy surgery centers record 19–23 channel EEG which makes this algorithm potentially

widely applicable, provided access to software is granted. The method could however also be applied to high-density EEG. While a vast majority of studies applying ICA to ictal EEG rely on low-density EEG, two studies [14, 15] proposed to apply ICA to 32 and 76 electrodes recordings and demonstrated that ICA utility is not limited to small numbers of electrodes. In that case, the reduction in the number of components to analyze becomes even more interesting since it could become excessively time-consuming to analyze each of the numerous components returned by ICA.

From an engineering point of view, the component selection step of the pipeline can be seen as a typical machine learning task: either of regression if the goal is to predict the distance to the resection zone for each component or of classification if we only want to know whether a component is accurate or not. Thanks to the quantitative measures that were implemented, it became possible to train a model in a supervised fashion. However, a challenge in the present study and in extratemporal lobe epilepsy studies, in general, is the limited amount of data showing a reliable *ground truth*, due to the lower rates of performed surgeries (temporal lobe epilepsy surgeries remain by far more frequent) and of its success in rendering seizure-free the patients (50%–60% [40, 41]). In this study, a leave-one-out validation was performed to avoid overestimating the performance of the proposed selection assistance with new data. Moreover, the complexity of the implemented technique is low, with only 3 parameters (i.e. the thresholds used to reject components) which have an intuitive interpretation, unlike the parameters of most machine learning models subject to overfitting. In this study, we avoided proposing a black-box technique and kept the methodology transparent and understandable without advanced expertise in machine learning. By implementing additional features, more sophisticated models (e.g. support vector machine) could be trained but, in that case, a larger database will likely be needed due to the increasing number of parameters and their lack of interpretability.

5. Conclusions

This study extends the work proving ICA efficiency to analyze ictal EEG, and adds new evidence of its utility for extratemporal lobe epilepsy. Quantitative measures were implemented to define a set of features characterizing ictal components, which might assist their recognition in a real-life clinical setting. A component selection assistance was proposed based on these features to help a clinician in his/her choice for ictal components. Further studies are warranted to explore the analyzed features as potential classifiers to automatize the best ictal component selection.

Data availability statement

The data generated and/or analysed during the current study are not publicly available for legal/ethical reasons but are available from the corresponding author on reasonable request.

Acknowledgments

This work was supported by the Fonds de la Recherche Scientifique—FNRS and the Fonds Wetenschappelijk Onderzoek—Vlaanderen under EOS Project No. 30468160. The work was also supported by the Fonds de Recherche Clinique des Cliniques Universitaires Saint-Luc and the Fondation Saint-Luc. SV is a Research Fellow 'Aspirant' funded by F.R.S.-FNRS (Fonds National de la Recherche Scientifique, Belgium).

ORCID iDs

Aurélie de Borman https://orcid.org/0000-0002-6730-0775
Simone Vespa https://orcid.org/0000-0002-0896-8142
P.-A. Absil https://orcid.org/0000-0003-2946-4178

References

[1] Xue-Ping W, Hai-Jiao W, Li-Na Z, Xu D and Ling L 2019 Risk factors for drug-resistant epilepsy: a systematic review and meta-analysis *Medicine* **98** e16402
[2] Ryvlin P and Rheims S 2008 Epilepsy surgery: eligibility criteria and presurgical evaluation *Dialogues Clin. Neurosci.* **10** 91–103
[3] Rosenow F 2001 Presurgical evaluation of epilepsy *Brain* **124** 1683–700
[4] Noachtar S and Rémi J 2009 The role of EEG in epilepsy: a critical review *Epilepsy Behav.* **15** 22–33
[5] Duez L *et al* 2019 Electromagnetic source imaging in presurgical workup of patients with epilepsy *Neurology* **92** e576–86
[6] LeVan P, Urrestarazu E and Gotman J 2006 A system for automatic artifact removal in ictal scalp EEG based on independent component analysis and Bayesian classification *Clin. Neurophysiol.* **117** 912–27
[7] Urrestarazu E, Iriarte J, Alegre M, Valencia M, Viteri C and Artieda J 2004 Independent component analysis removing artifacts in ictal recordings *Epilepsia* **45** 1071–8
[8] Urigüen J A and Garcia-Zapirain B 2015 EEG artifact removal—state-of-the-art and guidelines *J. Neural. Eng.* **12** 031001
[9] Iriarte J, Urrestarazu E, Artieda J, Valencia M, LeVan P, Viteri C and Alegre M 2006 Independent component analysis in the study of focal seizures *J. Clin. Neurophysiol.* **23** 551–8
[10] Nam H, Yim T-G, Han S K, Oh J-B and Lee S K 2002 Independent component analysis of ictal EEG in medial temporal lobe epilepsy *Epilepsia* **43** 160–4
[11] Leal A J R, Dias A I and Vieira J P 2006 Analysis of the EEG dynamics of epileptic activity in gelastic seizures using decomposition in independent components *Clin. Neurophysiol.* **117** 1595–601
[12] Jung K-Y, Kang J-K, Kim J H, Im C-H, Kim K H and Jung H-K 2009 Spatiotemporospectral characteristics of

scalp ictal EEG in mesial temporal lobe epilepsy with hippocampal sclerosis *Brain Res.* **1287** 206–19
[13] Leal A J R, Dias A I, Vieira J P, Moreira A, Távora L and Calado E 2008 Analysis of the dynamics and origin of epileptic activity in patients with tuberous sclerosis evaluated for surgery of epilepsy *Clin. Neurophysiol.* **119** 853–61
[14] Yang L, Wilke C, Brinkmann B, Worrell G A and He B 2011 Dynamic imaging of ictal oscillations using non-invasive high-resolution EEG *NeuroImage* **56** 1908–17
[15] Lu Y, Yang L, Worrell G A, Brinkmann B, Nelson C and He B 2012 Dynamic imaging of seizure activity in pediatric epilepsy patients *Clin. Neurophysiol.* **123** 2122–9
[16] Habib M A, Ibrahim F, Mohktar M S, Kamaruzzaman S B and Lim K S 2020 Recursive independent component analysis (ICA)-decomposition of ictal EEG to select the best ictal component for EEG source imaging *Clin. Neurophysiol.* **131** 642–54
[17] Foldvary N, Klem G, Hammel J, Bingaman W, Najm I and Lüders H 2001 The localizing value of ictal EEG in focal epilepsy *Neurology* **57** 2022–8
[18] de Borman A 2021 Estimation of seizure onset zone from ictal EEG using independent component analysis and source imaging *Master Thesis* Ecole polytechnique de Louvain, Université catholique de Louvain
[19] Homan R W 1988 The 10–20 electrode system and cerebral location *Am. J. EEG Technol.* **28** 269–79
[20] Wieser H G, Blume W T, Fish D, Goldensohn E, Hufnagel A, King D, Sperling M R and Lüders H 2003 Proposal for a new classification of outcome with respect to epileptic seizures following epilepsy surgery *Epilepsia* **42** 282–6
[21] Delorme A and Makeig S 2004 EEGLAB: an open source toolbox for analysis of single-trial EEG dynamics including independent component analysis *J. Neurosci. Methods* **134** 9–21
[22] Fatourechi M, Bashashati A, Ward R K and Birch G E 2007 EMG and EOG artifacts in brain computer interface systems: a survey *Clin. Neurophysiol.* **118** 480–94
[23] Winkler I, Debener S, Muller K-R and Tangermann M 2015 On the influence of high-pass filtering on ICA-based artifact reduction in EEG-ERP *2015 37th Annual Int. Conf. IEEE Engineering in Medicine and Biology Society (EMBC)* (Milan: IEEE) pp 4101–5
[24] Bertrand O, Perrin F and Pernier J 1985 A theoretical justification of the average reference in topographic evoked potential studies *Electroencephalogr. Clin. Neurophysiol./Evoked Potentials Section* **62** 462–4
[25] Onton J, Westerfield M, Townsend J and Makeig S 2006 Imaging human EEG dynamics using independent component analysis *Neurosci. Biobehav. Rev.* **30** 808–22
[26] Hyvärinen A and Oja E 2000 Independent component analysis: algorithms and applications *Neural Netw.* **13** 411–30
[27] Lee T-W 1998 *Independent Component Analysis: Theory and Applications* (Dordrecht: Kluwer Academic Publishers)
[28] Comon P 1994 Independent component analysis. A new concept? *Signal Process.* **36** 287–314
[29] Bell A J and Sejnowski T J 1995 An information-maximization approach to blind separation and blind deconvolution *Neural Comput.* **7** 1129–59
[30] Lee T-W, Girolami M and Sejnowski T J 1999 Independent component analysis using an extended infomax algorithm for mixed subgaussian and supergaussian sources *Neural Comput.* **11** 417–41
[31] Pascual-Marqui R D 2007 Discrete, 3D distributed, linear imaging methods of electric neuronal activity. Part 1: exact, zero error localization (https://doi.org/10.1016/j.clinph.2006.09.007)
[32] Pascual-Marqui R D *et al* 2011 Assessing interactions in the brain with exact low-resolution electromagnetic tomography *Phil. Trans. R. Soc.* A **369** 3768–84
[33] Presti P 2018 paolop21/simulation_source_connectivity (available at: https://github.com/paolop21/simulation_source_connectivity) (https://doi.org/10.1590/1806-9282.64.02.133) (accessed17 November 2020)
[34] Anzolin A, Presti P, van de Steen F, Astolfi L, Haufe S and Marinazzo D 2019 Quantifying the effect of demixing approaches on directed connectivity estimated between reconstructed EEG sources *Brain Topogr.* **32** 655–74
[35] Huang Y, Parra L C and Haufe S 2016 The New York Head—a precise standardized volume conductor model for EEG source localization and tES targeting *NeuroImage* **140** 150–62
[36] Fergus P, Hignett D, Hussain A, Al-Jumeily D and Abdel-Aziz K 2015 Automatic epileptic seizure detection using scalp EEG and advanced artificial intelligence techniques *Biomed. Res. Int.* **2015** 986736
[37] Friston K 2007 *Statistical Parametric Mapping: The Analysis of Functional Brain Images* W Penny, J Ashburner, S Kiebel, T Nichols and K Friston (New York: Academic Press)(https://doi.org/10.1016/B978-0-12-372560-8.X5000-1)
[38] Rorden C and Brett M 2000 Stereotaxic display of brain lesions *Behav. Neurol.* **12** 421719
[39] Siddiqui M K, Morales-Menendez R, Huang X and Hussain N 2020 A review of epileptic seizure detection using machine learning classifiers *Brain Inf.* **7** 5
[40] Englot D J, Breshears J D, Sun P P, Chang E F and Auguste K I 2013 Seizure outcomes after resective surgery for extra–temporal lobe epilepsy in pediatric patients: a systematic review *J. Neurosurg.: Pediatr.* **12** 126–33
[41] Englot D J and Chang E F 2014 Rates and predictors of seizure freedom in resective epilepsy surgery: an update *Neurosurg. Rev.* **37** 389–405